Proceedings of ISFOG 2025
5TH INTERNATIONAL SYMPOSIUM ON
FRONTIERS IN OFFSHORE GEOTECHNICS
Nantes, France | June 9-13 2025

ISBN 978-2-85782-758-0

Experimental analysis of the response of open-ended pipe piles to static and cyclic axial loading using digital image correlation

D. G. Fridman, M. Prezzi*, R. Salgado
Purdue University, West Lafayette, IN, United States
mprezzi@ecn.purdue.edu

ABSTRACT: Offshore foundation elements are often subjected to cycles of compressive and tensile loading. Open-ended pipe piles are frequently used as foundations for wind turbines as monopiles or as part of jacket structures. This paper reports the results of two open-ended pipe pile tests in a half-cylindrical calibration chamber with image analysis capabilities. The model piles, with diameters of 44 mm and 63 mm, were jacked into dense silica sand samples, statically load tested in compression, cyclically load tested (under displacement-controlled conditions), and statically load tested in compression a second time. The cyclic load tests had 100 cycles with a half-amplitude of 1 mm. Digital images captured during testing were analysed using digital image correlation to obtain the displacement fields in the soil domain. Image analyses of compressive static load tests indicate that the soil plug undergoes vertical compression during static loading. Cyclic loading leads to shaft resistance degradation, which is correlated with contractive radial strains around the model pile. Cycling also causes vertical compression below the pile base and inside the soil plug, which increases the base resistance of the piles and ultimately increases the total compressive capacity of the model open-ended piles under static loading.

Keywords: Open-ended pipe piles; axial loading; cyclic loading; digital image correlation

1 INTRODUCTION

Open-ended pipe piles (OEPs) are widely used in offshore applications, such as wind turbines and oil production platforms. Offshore OEPs can be installed as a single, large-diameter pile, typically called monopile; they are also frequently used as foundation elements of jacket structures. When jacket structures support offshore wind turbines or other light offshore structures, the nature of the loads they experience, combined with the low self-weight of the structures, frequently leads to cycles of compressive and tensile axial loads acting on the OEPs (Gavin et al., 2011).

Both OEPs and closed-ended pipe piles (CEPs) subjected to cyclic loading tend to undergo shaft resistance degradation (Igoe et al., 2011; D. White & Deeks, 2007; D. J. White & Lehane, 2004), which decreases their shaft capacity. This phenomenon has been widely explored, especially regarding the tensile capacity of a pile (Jardine & Standing, 2012). While the tensile capacity of a pile is derived from shaft resistance only, the compressive capacity also depends on unit base resistance q_b. Galvis-Castro et al. (2023) used calibration chamber experiments to show that, for larger cyclic displacement half-amplitudes (≈ 0.1 diameter), the q_b of CEPs may increase after cycling. Wang et al. (2021) also observed that the q_b increased after cycling in centrifuge tests, and Puech (2013) and Keefe et al. (2020) reported an increase in pile compressive capacity after cycling in CEP and OEP field tests, respectively. Comprehensive analyses of pile-soil interaction are needed to provide a better understanding of how the pile capacity to axial loading changes with cycling.

Digital image correlation (DIC) uses images of the soil domain captured during testing to calculate displacement and strain fields caused by pile movement. It has been extensively used for cone penetration tests and model CEPs (Arshad et al., 2014; Galvis-Castro et al., 2023), and recently also for OEPs (Fridman et al., 2025; Prezzi et al., 2025).

This paper presents the results of two model OEP tests, including compressive static load tests and cyclic load tests, performed in a half-cylindrical calibration chamber with image analysis capabilities. We present load measurements and displacement and strain fields in the soil domain for both static and cyclic load tests. Using image analysis, we assess how deformation in the soil domain during cycling influences the load transfer mechanism of the model OEPs.

2 MATERIALS AND METHODS

Two model OEPs were installed in a half-cylindrical calibration chamber with visualization windows (see Figure 1). The model piles had diameter B = 44 mm and 63 mm and wall thickness t = 9.5 mm and 12.7 mm, respectively. More details about the calibration chamber and the model piles can be found in Arshad (2014), Fridman et al., (2025), and Tovar-Valencia et al., (2023). The sand used in this study was Ottawa 20-30, a poorly graded silica sand with mean particle diameter D_{50} = 0.72 mm. For each model OEP test, a fresh dense sample with relative density $D_R \approx 90\%$ was prepared using air pluviation. Each test consisted of four stages: (1) installation by jacking, (2) compressive static load test, (3) displacement-controlled cyclic load test, and (4) compressive static load test after cycling. The model piles were preinstalled to a depth of 22 mm to ensure alignment with the glass; then, they were jacked to a depth of 374 mm from the ground surface at a rate of 1 mm/s. The first static load test was performed at a rate of 0.1 mm/s to a maximum displacement of 13 mm. The displacement-controlled cyclic load test was performed with a half-amplitude Δw of 1 mm, frequency f of 0.1 Hz and number of cycles N of 100. The second static load test was performed at a rate of 0.1 mm/s to a maximum displacement of 25 mm. During testing, a load cell attached to the pile head measured the total load applied on the model OEP. High-resolution digital cameras captured images of the test at a rate of 2 frames per second for installation and static load tests and 4 frames per second for cyclic tests. After testing, the test images were analysed using digital image correlation (DIC) to obtain the displacements and strains in the soil domain.

3 INSTALLATION AND STATIC LOAD TEST

Figure 2(a) shows the jacking resistance for both tests. The jacking resistance increased with depth during both installations; the 63-mm-pile reached a maximum jacking resistance of 1,831 N at the final depth, while the 44-mm-pile reached a maximum jacking resistance of 1,166 N at the final depth. Figure 2(b) shows the load-displacement curve for the compressive static load tests performed after pile installation. Both model OEPs plunged before reaching a pile head displacement of 0.1B. The maximum loads in the load tests were similar to the loads measured at the end of pile installation.

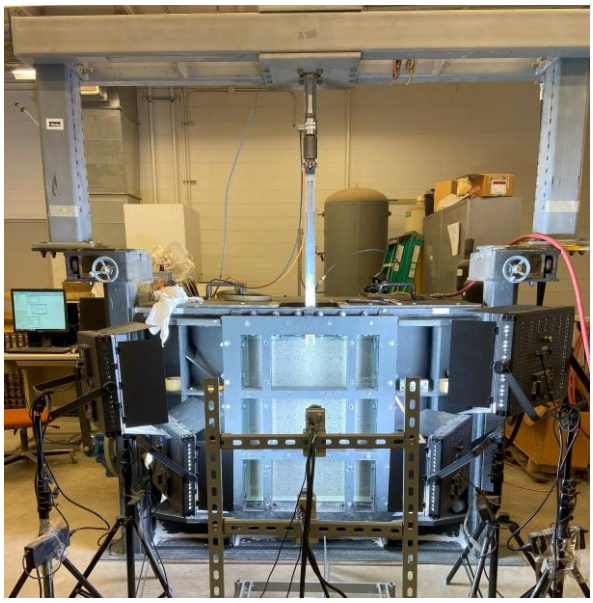

Figure 1. Calibration chamber at Purdue University

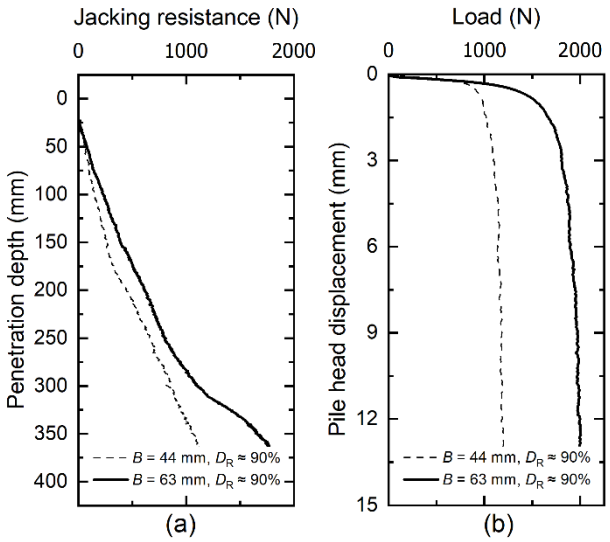

Figure 2. Load measurements during installation and loading: (a) jacking resistance and (b) load versus pile head displacement for the first load test

Figure 3 shows the vertical displacement increments du_z in the soil domain after a 5-mm pile head displacement during static loading. Positive du_z represents upward movement and negative du_z represents downward movement. The radial position r in the horizontal axis and the vertical position h in the vertical axis are normalised by the pile radius r_p. In Figure 3, the maximum magnitude of du_z during loading is located immediately under the pile annulus, where $du_z \approx$ -3.5 mm, with a bulb of smaller magnitude (< -0.6 mm) under the entire pile base. Outside the pile shaft, some upward movement was observed due to the dilative nature of the dense sand and the low confinement levels. The entire soil plug moved downward, but inside the plug there were

different magnitudes of du_z. Near the plug base, $du_z \approx 0$ mm; at a height of $1B$ above that, $du_z \approx$ -0.4 mm; and, at the top of the soil plug, $du_z \approx$ -0.6 mm. These displacement increments indicate vertical compression of the OEP plug during static loading. Field OEPs are typically believed to fail in fully plugged mode during static compressive loading because field measurements showed that the top of the plug moves with the OEP as it is displaced downward (Paikowsky et al., 1989; Randolph et al., 1991). The image analysis of the soil plug during compressive static loading (Figure 3) suggests that these previous observations would also be consistent with some soil entering the pile shaft, with plug compression compensating for that, so that the top of the plug remains stationary with respect to the pile.

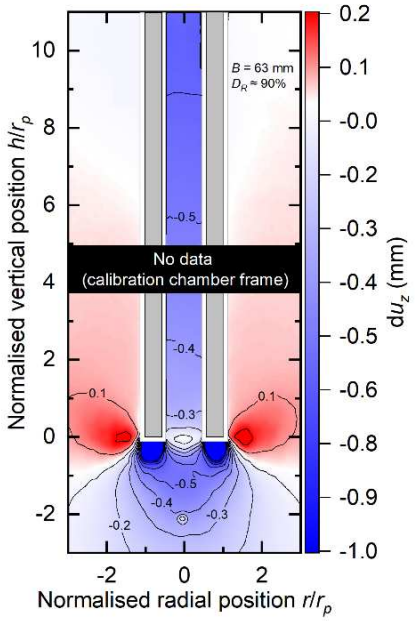

Figure 3. Vertical displacement field during loading for a pile head displacement increment of 5 mm

4 CYCLIC LOAD TESTS

Figure 4 shows the loads measured during cyclic loading and the pile head displacement w for the 44-mm model OEP and the 63-mm model OEP installed in dense samples. Positive loads are compressive, negative loads are tensile; the values of w are positive for downward pile head movement and negative for upward pile head movement. For both tests, the maximum compressive load $Q_{c,1}$ measured in the first cycle was similar to the load measured at the end of the static load test (1,161 N for the 44-mm pile and 1,990 N for the 63-mm pile). After that, both tests had a sharp decrease in maximum compressive load Q_c during the first six cycles to 0.30-0.35$Q_{c,1}$. As the model OEP continued cycling, Q_c slowly increased with each cycle to 0.44$Q_{c,1}$ at N = 100 for both diameters. This behaviour in compressive loading during displacement-controlled cyclic loading, with a sharp drop followed by a slow, steady increase in resistance is likely explained by the base resistance q_b of the OEP (Galvis-Castro et al., 2023). Galvis-Castro et al. (2023) reported a curve of similar geometry for model CEPs that were cyclically load tested with $\Delta w \approx 0.1B$, which seems to be consistent with $\Delta w \approx 0.1t$ for OEPs. The tensile load when the pile was pulled upwards was maximum during the first cycle and stabilised after nine cycles, indicating some shaft resistance degradation. This will be further explored with the use of DIC.

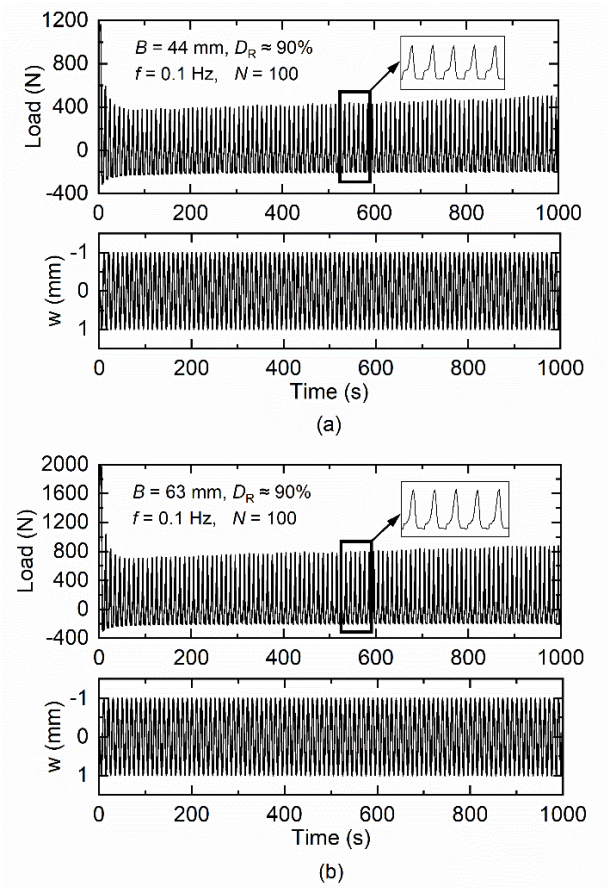

Figure 4. Loads and displacements measured during cyclic loading: (a) 44-mm model OEP and (b) 63-mm model OEP

Figure 5 shows the total displacement and strain fields in the sand domain from the start of cycling to the time corresponding to 100 load cycles of the 63-mm model OEP. The final position of the model pile at N = 100 was the same as at N = 0. Figure 5(a) shows the total displacement u represented by equally spaced vectors. Figure 5(b) and (c) show the displacement fields (radial displacement u_r and vertical displacement u_z), and Figure 5(d) and (e) show the strain fields (radial strains E_{rr} and vertical

strains E_{zz}) in the soil around the pile. For the strains, negative signs indicate contraction, while positive signs indicate extension. The displacement vectors in Figure 5(a) show that the largest displacements in the sand domain (> 10 mm) were inside the model OEP plug. The plug was not only displaced downward as the soil below the pile base was pushed down, but it also underwent compression, similarly to what happened in the static load test. The vertical displacement contour plot [Figure 5(b)] shows that u_z at the plug base level was -5 mm, while u_z = -15 mm near the top of the plug. The sand leaving the plug causes the displacement paths under the annulus and immediately outside the pile shaft to have a curved pattern around the pile annulus, with vectors of greater magnitude where $|r|/r_p < 1$ and $h/r_p > -1$.

In Figure 5(c), the greatest values of u_r (u_r = 2.5 mm) are located under the pile annulus, with sand being displaced towards the outside of the pile. Inside the plug, near its base, the sand was also displaced in that direction, towards the inner walls.

The magnitudes of the vertical strains in Figure 5(d) are maximum under the pile annulus and at the plug base. The sand at the plug base was vertically compressed during cycling, resulting in E_{zz} = 15%. This also explains the proximity between the u_z contour lines near the plug base in Figure 5(b). In the same region, Figure 5(e) shows that the sand was radially extended with E_{rr} = 15%. As mentioned previously, the soil plug underwent vertical compression: the entire plug has negative values of E_{zz}, ranging from -15% to 0%, with magnitudes varying across the length of the plug. In Figure 5(e), there are negative radial strains of magnitude near 1% around the outer walls of the model OEP. This radial contraction of the sand around the pile shaft decreases the radial stresses acting on the pile walls (Galvis-Castro, 2020). This decrease in radial stresses decreases the shaft resistance that the pile can mobilise, a process to which we refer as shaft resistance degradation. This is also illustrated in Figure 5(c), in which the sand around the pile shaft ($|r|/r_p > 1$ and $h/r_p > 0$) moved slightly towards the pile outer walls. Finally, there is a region underneath the soil plug ($|r|/r_p < 0.5$ and $-1 < h/r_p < -0.5$) where both E_{rr} and E_{zz} are nearly zero after 100 cycles.

The displacement and strain fields in the sand domain around and inside the model OEP provide more insights into the mechanisms behind the implied shaft resistance degradation and increase in base resistance observed in the measurements of loads during the displacement-controlled cyclic load tests. The shaft resistance degradation is caused by a decrease in radial stresses around the pile outer walls, which is in turn caused by the contractive radial strains that are observed in those regions. The increase in base resistance is correlated with the downward vertical displacement of the soil inside the plug and under the pile base.

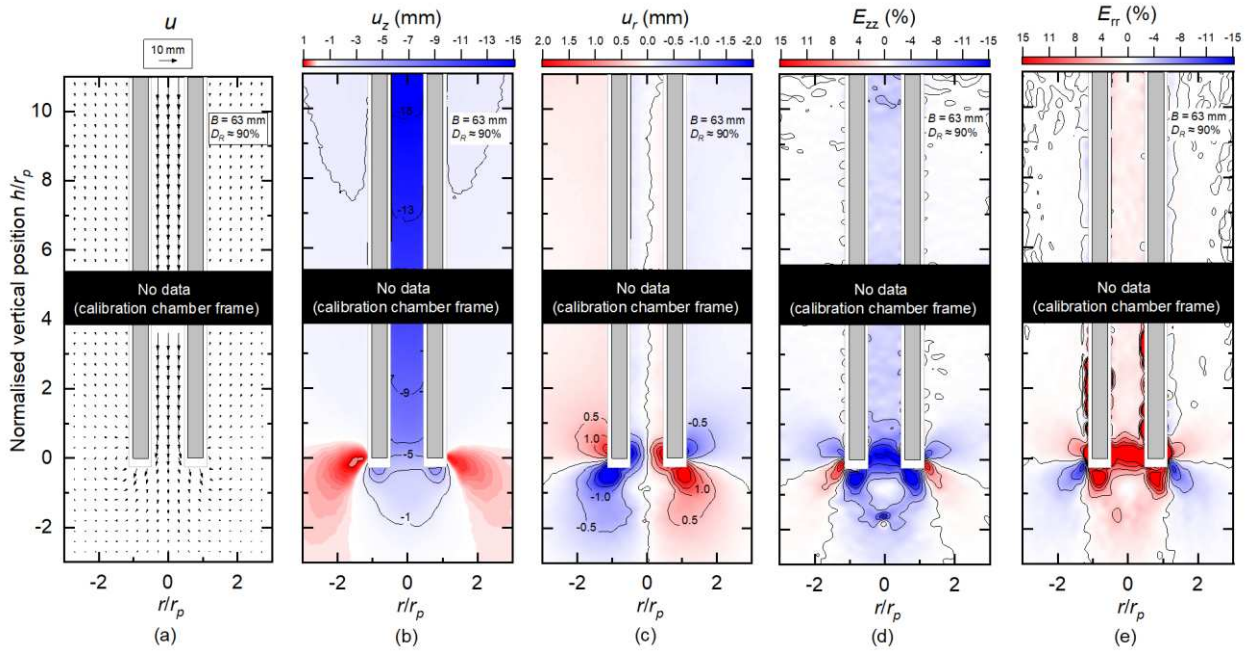

Figure 5. Vector and contour plots for a cumulative analysis of the cyclic load test after 100 cycles for B = 63 mm and D_R ≈ 90%: (a) displacement vectors, (b) vertical displacements, (c) radial displacements, (d) vertical strains, and (e) radial strains

5 EFFECT OF CYCLING IN PILE CAPACITY

Figure 6 shows a comparison of the curves of load versus pile head displacement during compressive static load tests before and after cycling for the 44-mm and the 63-mm model OEPs. Both model OEPs needed more pile head displacement (≈ 9 mm) to fully mobilise their capacities after cycling. However, both model OEPs sustained greater loads after cycling. In Figure 6(a), for a pile head displacement of 4.4 mm (0.1*B*), the load applied on the 44-mm model pile was 1,144 N before cycling and 1,180 N after cycling. In Figure 6(b), for a pile head displacement of 6.3 mm (0.1*B*), the load mobilised on the 63-mm model pile was 1,910 N before cycling and 2,107 N after cycling.

These larger pile head displacements needed to fully mobilise pile capacity after cycling are related to the base capacity. The shaft capacity of piles tends to be fully mobilised at small pile head displacements (≤ 0.01*B*), while full mobilisation of base capacity requires larger displacements (Salgado, 2022), especially after cycling compresses the zone underneath the pile base (Galvis-Castro et al., 2023). This is consistent with the image analysis in the previous section in suggesting that the model OEPs underwent shaft resistance degradation and an increase in q_b because of cyclic loading. Overall, for the test conditions in this study, cyclic loading of model OEPs resulted in an increase in static compressive capacity of up to 10% for a pile head displacement of 0.1*B*.

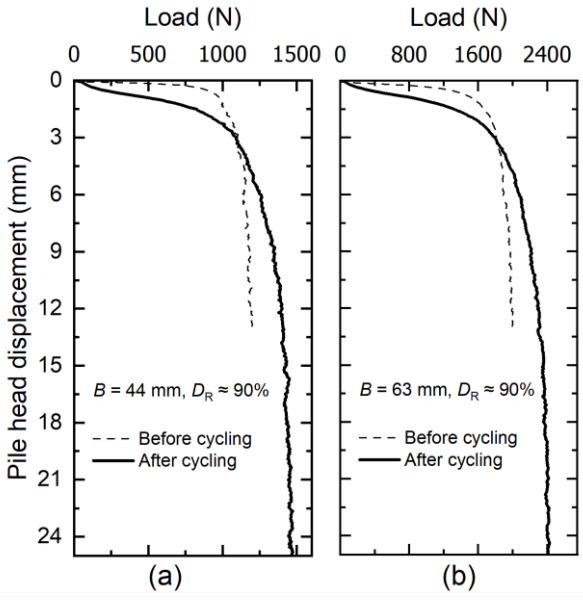

Figure 6. Comparison of load-displacement curves of compressive static load tests before and after cycling: (a) 44-mm model OEP and (b) 63-mm model OEP

6 CONCLUSIONS

Two model open-ended piles were installed in dense silica sand samples and the loaded in the following sequence: static compression, cyclic loading, and static compression again. This paper reported the loads measured during testing and presented results of image analysis of the sand domain using digital image correlation.

The plugs of the model OEPs underwent vertical compression under compressive static loading. This suggests that field OEPs that seem plugged during static loading may still allow some soil to enter the pile shaft, with vertical compression of the plug compensating the increase in mass to keep the top of the soil plug in place relative to the pile walls. Around the pile outer walls, contractive radial strains were consistent with shaft resistance degradation, which was also indirectly observed in load measurements.

Comparing the model pile capacities under compressive static loading before and after cycling, there was an increase of up to 10% in capacity for a pile head displacement of 0.1*B*. This increase in capacity is mainly due to an increase in the base resistance of the model OEP.

AUTHOR CONTRIBUTION STATEMENT

Daniel G. Fridman: Methodology, Investigation, Formal Analysis, Writing- original draft. **Monica Prezzi**.: Conceptualization, Funding acquisition, Supervision, Writing- Reviewing and Editing. **Rodrigo Salgado**: Conceptualization, Funding acquisition, Supervision, Writing- Reviewing and Editing.

ACKNOWLEDGEMENTS

This material is based upon work supported by the National Science Foundation under Grant No. 2028672. The authors are very grateful for this support. Any opinions, findings, and conclusions or recommendations expressed in this material are those of the author(s) and do not necessarily reflect the views of the National Science Foundation. The authors would also like to acknowledge the assistance of Gabriele Velloso in figure preparation.

REFERENCES

Arshad, M. I. (2014). *Experimental study of the displacements caused by cone penetration in*

sand. PhD thesis, Purdue University, West Lafayette, IN.

Arshad, M. I., Tehrani, F. S., Prezzi, M., & Salgado, R. (2014). Experimental study of cone penetration in silica sand using digital image correlation. *Geotechnique*, *64*(7), 551–569. https://doi.org/10.1680/geot.13.P.179

Fridman, D. G., Prezzi, M., & Salgado, R. (2025). Experimental study of plug formation in open-ended pipe piles using image analysis. *Ocean Engineering*, *327*, 120912. https://doi.org/10.1016/j.oceaneng.2025.120912

Galvis-Castro, A. C. (2020). *Investigation of monotonic and cyclic loading of piles in sand using a DIC calibration chamber*. PhD thesis, Purdue University, West Lafayette, IN. https://doi.org/10.25394/PGS.13337381.v1

Galvis-Castro, A. C., Tovar-Valencia, R. D., Prezzi, M., & Salgado, R. (2023). Effect of cyclic loading on the mobilization of unit base resistance of model piles jacked in sand. *Acta Geotechnica*, *18*(9), 4747–4766. https://doi.org/10.1007/s11440-023-01840-5

Gavin, K., Igoe, D., & Doherty, P. (2011). Piles for offshore wind turbines: A state-of-the-art review. *Proceedings of the Institution of Civil Engineers: Geotechnical Engineering*, *164*(4), 245–256. https://doi.org/10.1680/geng.2011.164.4.245

Igoe, D. J. P., Gavin, K. G., & O'Kelly, B. C. (2011). Shaft Capacity of Open-Ended Piles in Sand. *Journal of Geotechnical and Geoenvironmental Engineering*, *137*(10), 903–913. https://doi.org/10.1061/(asce)gt.1943-5606.0000511

Jardine, R. J., & Standing, J. R. (2012). Field axial cyclic loading experiments on piles driven in sand. *Soils and Foundations*, *52*(4), 723–736. https://doi.org/10.1016/j.sandf.2012.07.012

Keefe, T. E., Hussien, A. M., Bradshaw, A. S., Deeks, A. D., Rahim, A., Menq, F., & Gilbert, R. (2020). Cyclic axial load testing of pipe piles in sand. *4th International Symposium on Frontiers in Offshore Geotechnics (ISFOG 2020 in 2022)*, 529–540.

Paikowsky, S. G., Whitman, R. V., & Baligh, M. M. (1989). A new look at the phenomenon of offshore pile plugging. *Marine Geotechnology*, *8*(3), 213–230. https://doi.org/10.1080/10641198909379869

Prezzi, M., Sakleshpur, V. A., & Fridman, D. G. (2025). Installation Effects on the Capacity of Open-Ended and Closed-Ended Pipe Piles. In B. Indraratna & C. Rujikiatkamjorn (Eds.), *Recent Advances and Innovative Developments in Transportation Geotechnics* (pp. 17–29). Springer, Singapore. https://doi.org/10.1007/978-981-97-8245-1_2

Puech, A. (2013). Advances in axial cyclic pile design: contribution of the SOLCYP project. *ISSMGE Technical Committee TC 209—Offshore Geotechnics*, 45–57.

Randolph, M. F., Leong, E. C., & Houlsby, G. T. (1991). One-dimensional analysis of soil plugs in pipe piles. *Géotechnique*, *41*(4), 587–598. https://doi.org/10.1680/geot.1991.41.4.587

Salgado, R. (2022). *The Engineering of Foundations, Slopes and Retaining Structures*. CRC Press. https://doi.org/10.1201/b22079

Tovar-Valencia, R. D., Galvis-Castro, A., Salgado, R., Prezzi, M., & Fridman, D. (2023). Experimental measurement of particle crushing around model piles jacked in a calibration chamber. *Acta Geotechnica*, *18*(3), 1331–1351. https://doi.org/10.1007/s11440-022-01681-8

Wang, S., Lei, X., Meng, Q., Xu, J., Wang, M., & Guo, W. (2021). Model tests of single pile vertical cyclic loading in calcareous sand. *Marine Georesources and Geotechnology*, *39*(6), 670–681. https://doi.org/10.1080/1064119X.2020.1744048

White, D., & Deeks, A. (2007). Recent research into the behaviour of jacked foundation piles. *Proceedings of the International Workshop on Recent Advances in Deep Foundations*, *68*(1).

White, D. J., & Lehane, B. M. (2004). Friction fatigue on displacement piles in sand. *Géotechnique*, *54*(10), 645–658. https://doi.org/10.1680/geot.2004.54.10.645